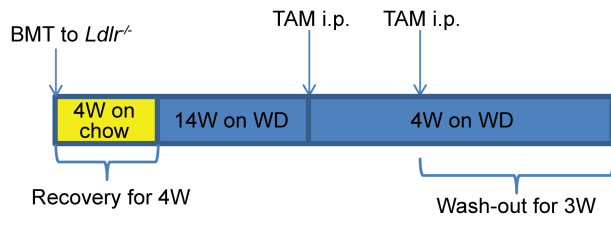
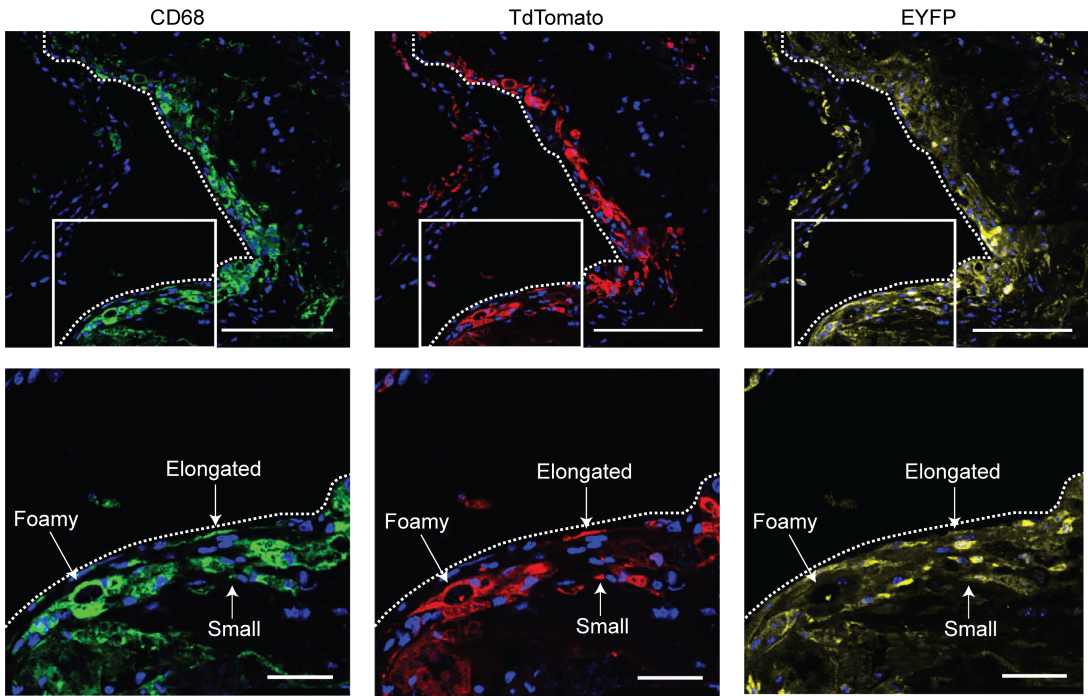


A



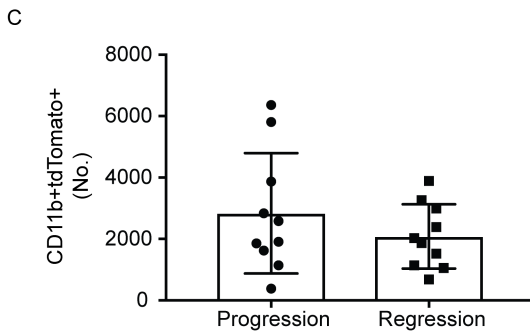
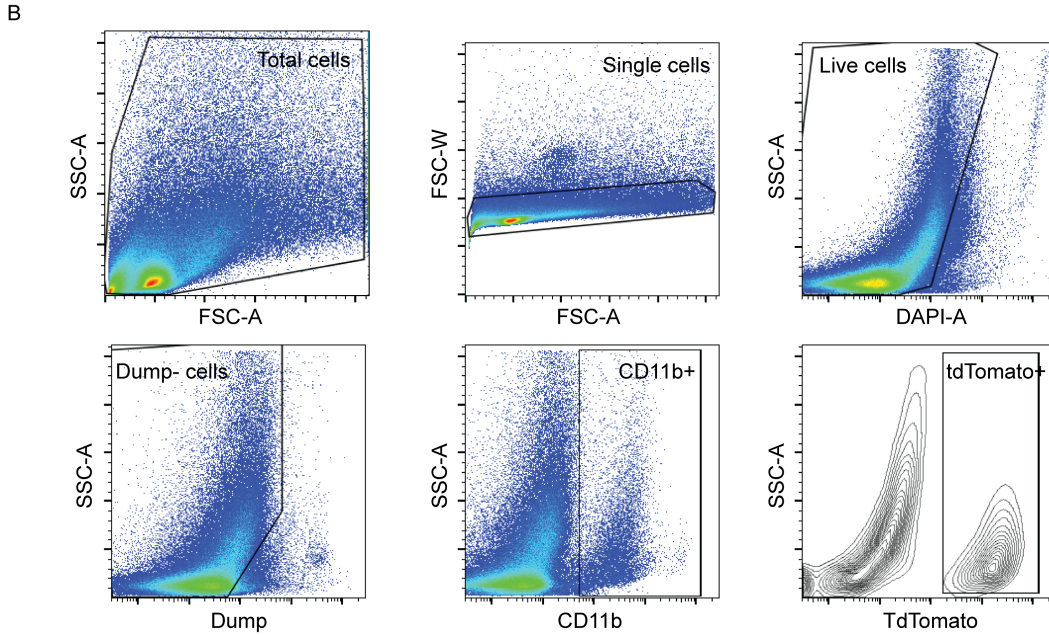
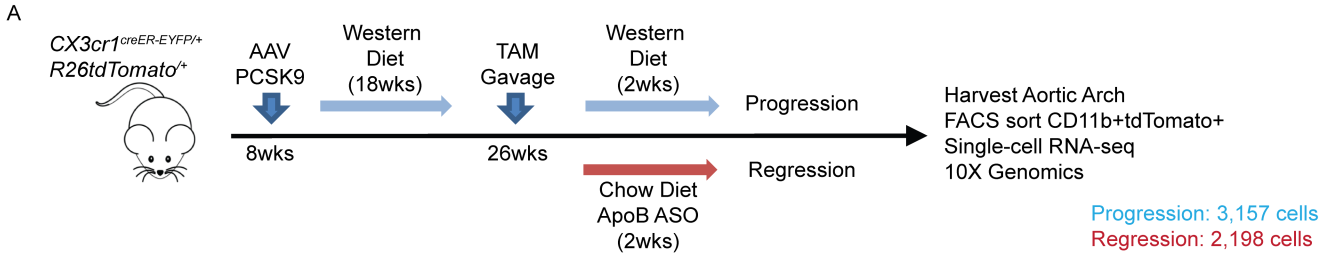
B



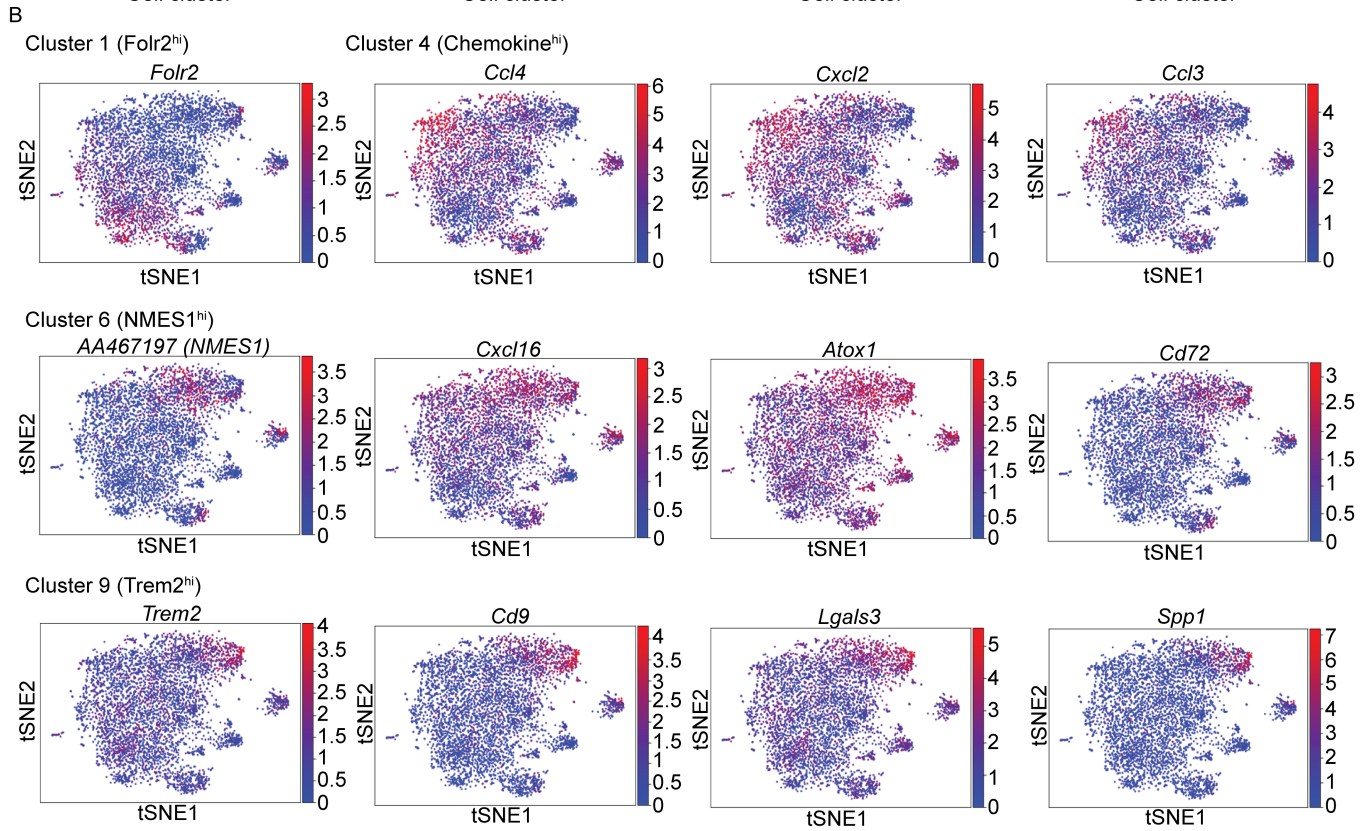
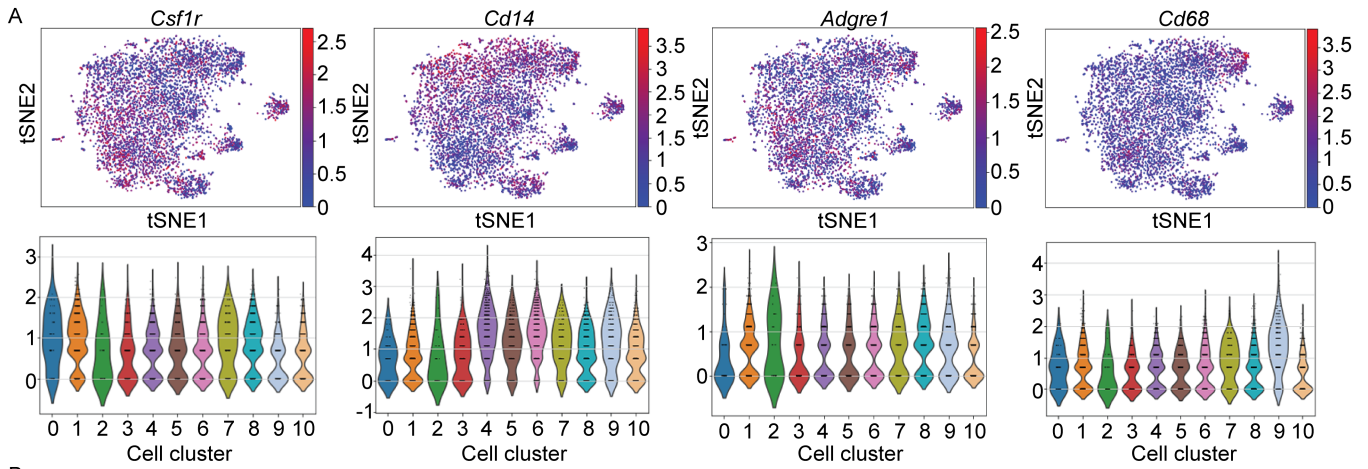
Supplemental Figure 1. Fate mapping the conversion of CX3CR1+ cells into plaque macrophages

in *Ldlr*^{-/-} : *Cx3cr1*^{CreERT2-IRES-YFP/+} *Rosa26*^{floxed-tdTomato/+} bone marrow chimeric mice during

atherosclerosis progression. (A) Schematic of the experimental atherosclerosis protocol using the model in *Ldlr*^{-/-} : *Cx3cr1*^{CreERT2-IRES-YFP/+} *Rosa26*^{floxed-tdTomato/+} bone marrow chimeric mice. Bone marrow from *Cx3cr1*^{CreERT2-IRES-YFP/+} *Rosa26*^{floxed-tdTomato/+} mice were transplanted into irradiated *Ldlr*^{-/-} mice, which were allowed to recover for 4 weeks on chow diet and were subsequently fed Western diet for 18 weeks. Mice were injected intra-peritoneal (i.p.) with tamoxifen (TAM) at week 14 and 15 after the switch to a Western diet to label CX3CR1+ derived cells. Mice were sacrificed 3 weeks later for analysis. **(B)** Representative confocal images of aortic roots stained for CD68 (green), EYFP (yellow), and TdTomato (red). Arrows point towards representative TdTomato+ cells with different phenotypes, including “slender and elongated”, “large and foamy” and “small” macrophages. Scale bar: 100um. Scale bar in zoomed in image: 50 um.

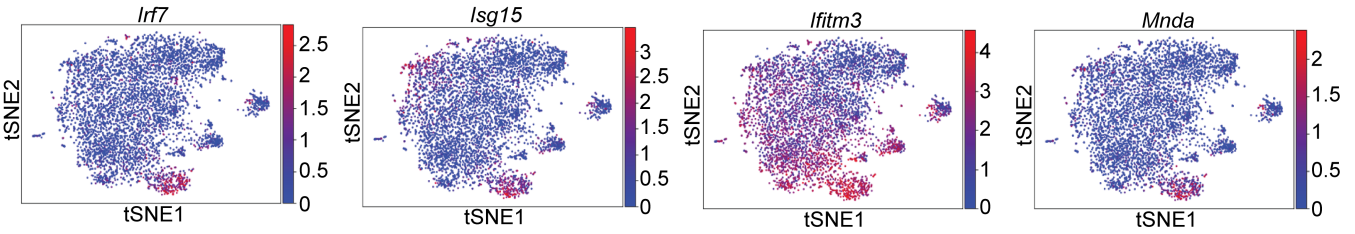


Supplemental Figure 2. Combining single cell RNA sequencing with genetic fate mapping to track and characterize cells derived from CX3CR1+ precursors during atherosclerosis progression and regression in *Cx3cr1*^{CreERT2-IRES-YFP/+}*Rosa26*^{flxed-tdTomato/+} mice. (A) Schematic of experimental protocol for single cell RNA-seq analyses of fate mapped cells during atherosclerosis progression and regression. *Cx3cr1*^{CreERT2-IRES-YFP/+}*Rosa26*^{flxed-tdTomato/+} mice (8 weeks old) were injected with AAVmPCSK9 and fed with Western Diet for 18 weeks. Cells derived from CX3CR1+ precursors were then labeled by tamoxifen (TAM) treatment by gavage. Mice were then divided to 2 groups: 1) a progression group, in which mice were continued on the Western diet for an additional 2 weeks, and 2) a regression group, in which mice were switched to chow and injected intraperitoneally with a apoB antisense oligonucleotide (ApoB-ASO; 50mg/kg; 2 doses/week; n=4 mice per group) for 2 weeks to lower plasma levels of atherogenic apoB-containing lipoproteins. The aortic arches were digested and FACS sorted for CD11b+TdTomo+ cells that were then subjected to single-cell RNA sequencing on the 10X genomics platform to profile 3,157 cells and 2,198 cells from progression and regression groups, respectively. (B) Gating and sorting strategies of aortic CD11b+TdTomo+ cells after excluding doublet, dead, and dumping gates from mice in *Cx3cr1*^{CreERT2-IRES-YFP/+}*Rosa26*^{flxed-tdTomato/+} mice for progression and regression group. (C) Absolute numbers of CD11b+TdTomo+ cells that were able to be FACS sorted from aortic arches of *Cx3cr1*^{CreERT2-IRES-YFP/+}*Rosa26*^{flxed-tdTomato/+} mice in progression and regression groups (n=10 per group, 3 individual experiments). Statistical significance was calculated using Student's *t* test and data are presented as mean ± SEM.

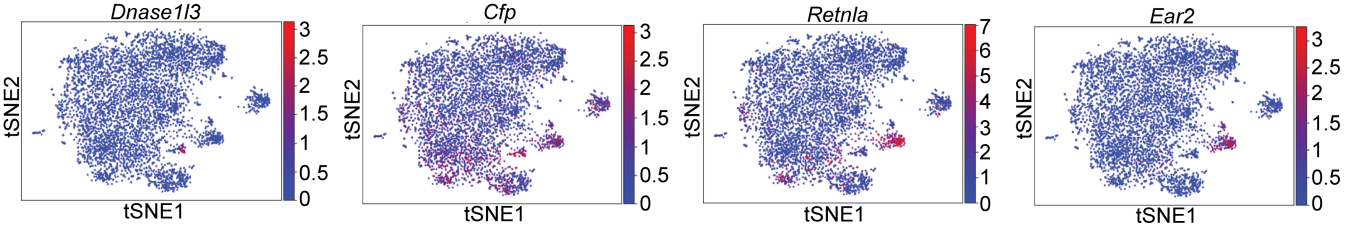


Supplemental Figure 3. Gene ranking and expression features from indicated cell clusters. (A) t-SNE plots of sorted CD11b+TdTomo+ cells colored based on expression of *Csflr*, *Cd14*, *Adgre1*, and *Cd68* genes, with corresponding violin plots below showing the expression level of each gene in the indicated cell clusters described in Figure 2. **(B)** t-SNE plots colored based on expression of most highly upregulated genes for Cluster1, Cluster4, Cluster6 and Cluster9 (shades of red indicate higher gene counts per cell).

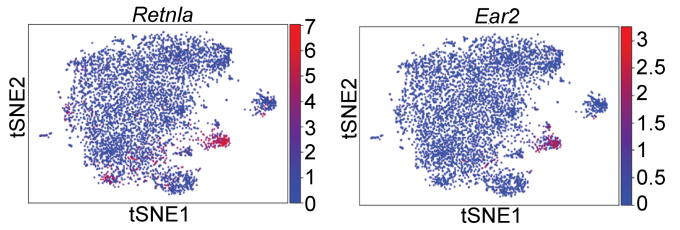
Cluster 5 (IFN signature^{hi})



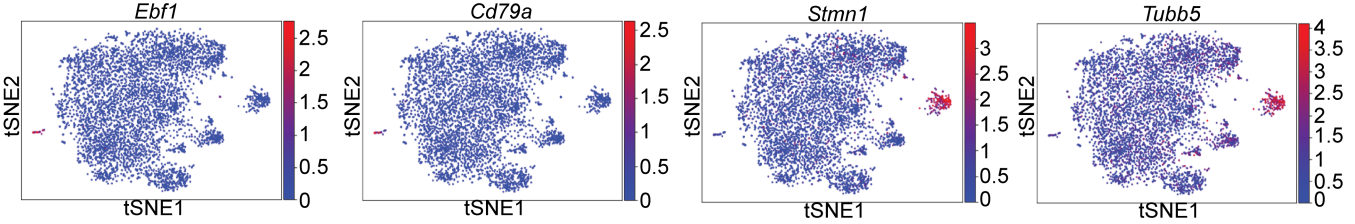
Cluster 0 (Dnase113^{hi})



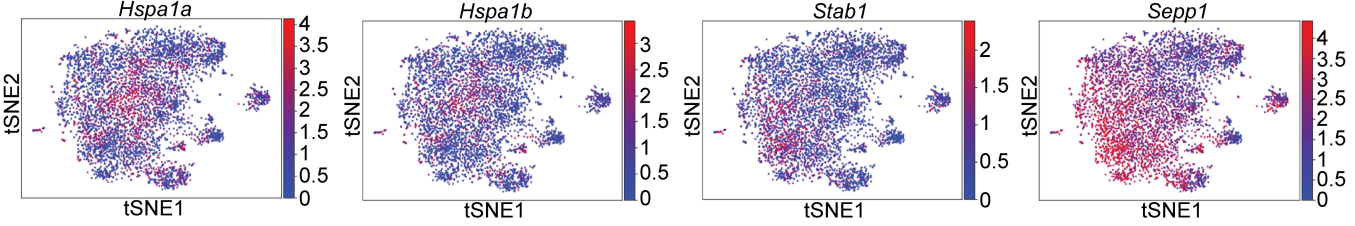
Cluster 3 (Retnla^{hi}Ear2^{hi})



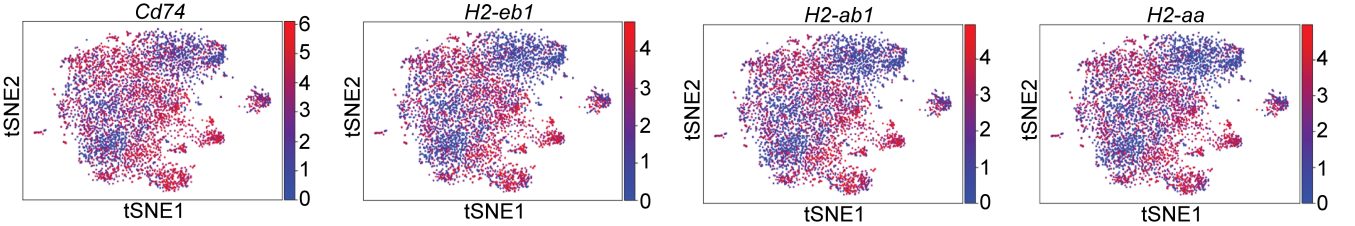
Cluster 2 (Ebf1^{hi}Cd79a^{hi})



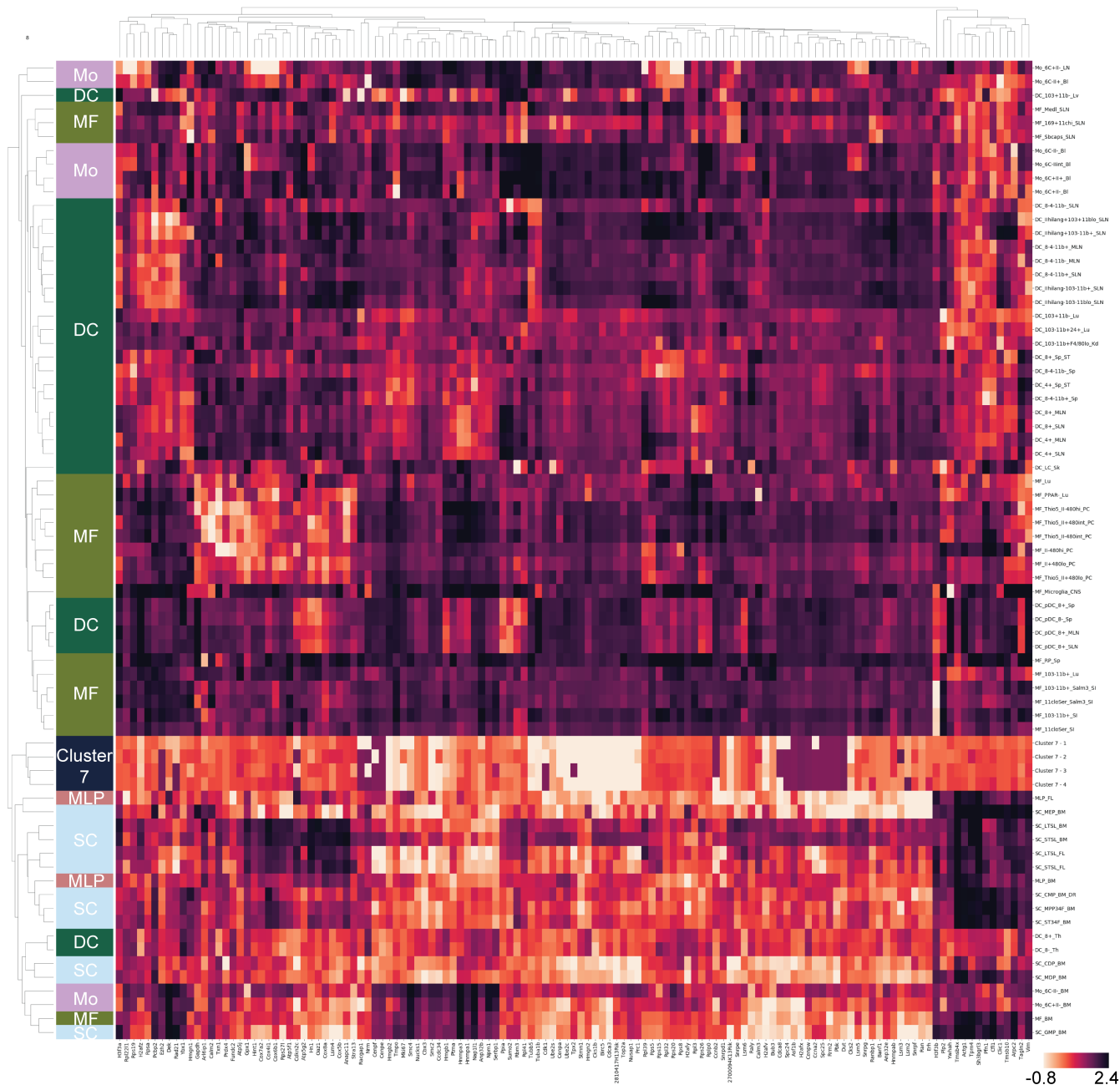
Cluster 8 (HSP^{hi})



Cluster 10 (Cd74^{hi}MHCII^{hi})



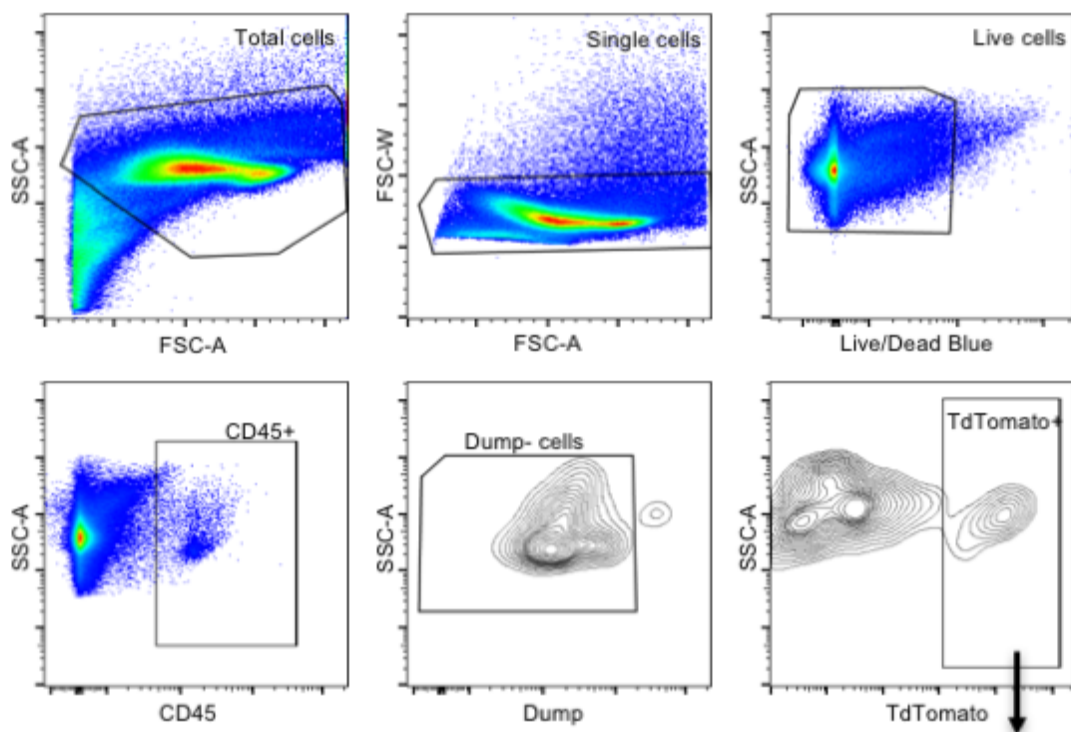
Supplemental Figure 4. Gene expression features from indicated cell clusters. t-SNE plots colored based on expression of most highly upregulated genes for the indicated cell Clusters (shades of red indicate higher gene counts per cell).



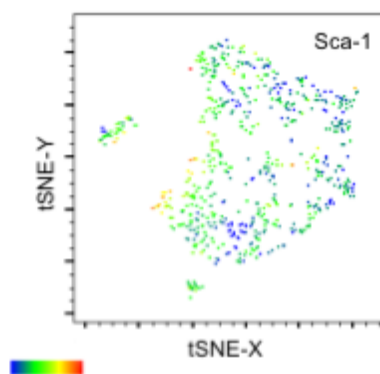
-0.8 2.4

Supplemental Figure 5. Comparing the transcriptional profile of the stem-like Cluster 7 with the IMMGEN database. 138 genes that were expressed >1 read in 90% of cells in Cluster 7 were compared to the gene expression of macrophages, monocytes, myeloid progenitors, stem cells and dendritic cells as extracted from the IMMGEN database. Cells from Cluster 7 were randomly grouped into four subgroups (shown in black) and median expression of each gene is shown. The heatmap illustrates the clustering of similar cell types and genes based on normalized gene expression profiles.

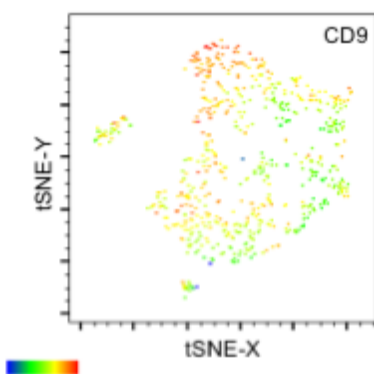
A



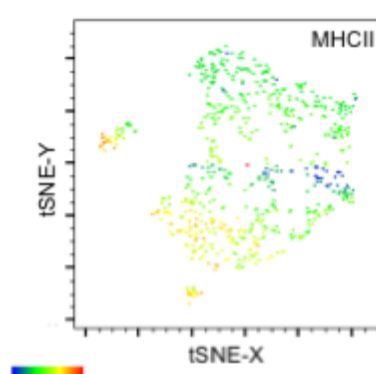
B



C



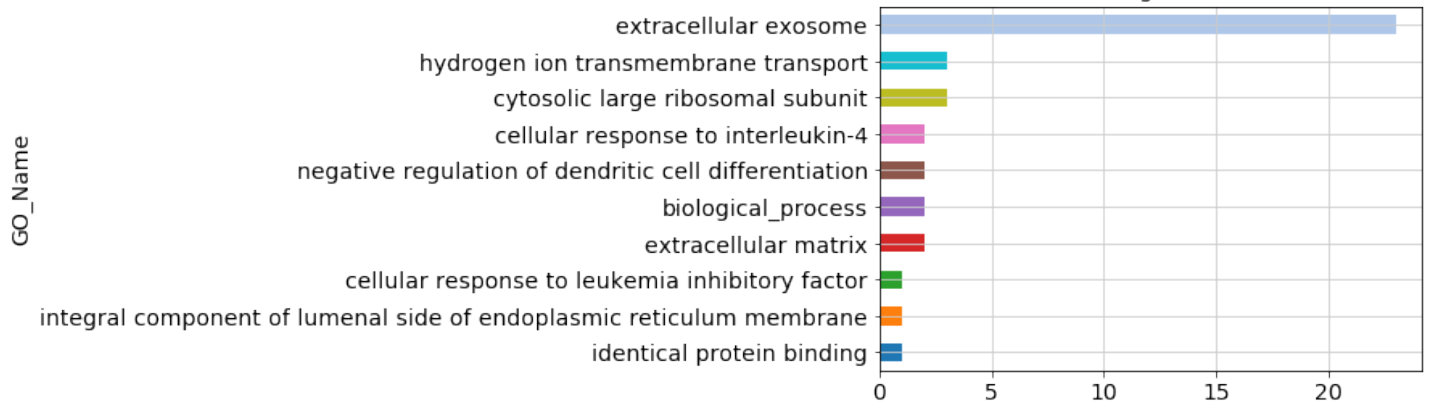
D



Supplemental Figure 6. FACS analysis of marker genes from Clusters in plaque macrophages derived from CX3CR1+ monocyte precursors in atherosclerosis progression. The aortic arches from the progression group (n=3) were digested and FACS analyzed for CD45+CD11b+TdTomato+ cells. **(A)** Representative gating strategies of aortic CD45+CD11b+TdTomato+ cells after excluding doublet, dead, and dumping gates. **(B)** t-SNE analysis of CD45+CD11b+TdTomato+ cells for expression of Sca-1 (Ly6a/e), **(C)** CD9, and **(D)** MHCII.

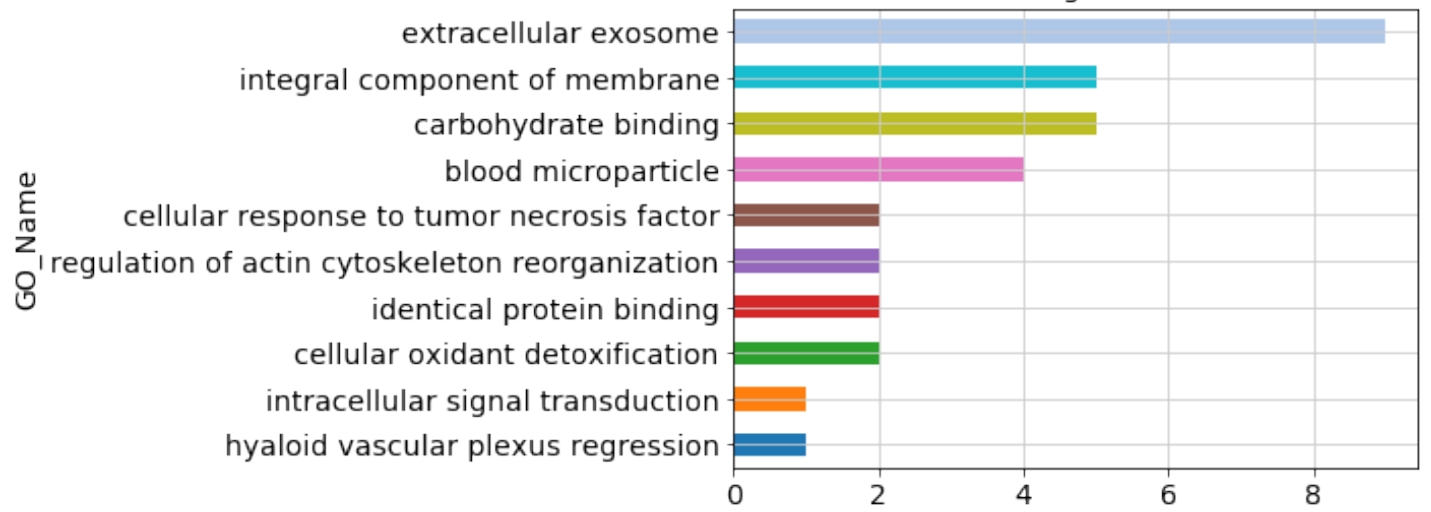
A

Enriched Ontologies in Cluster #0



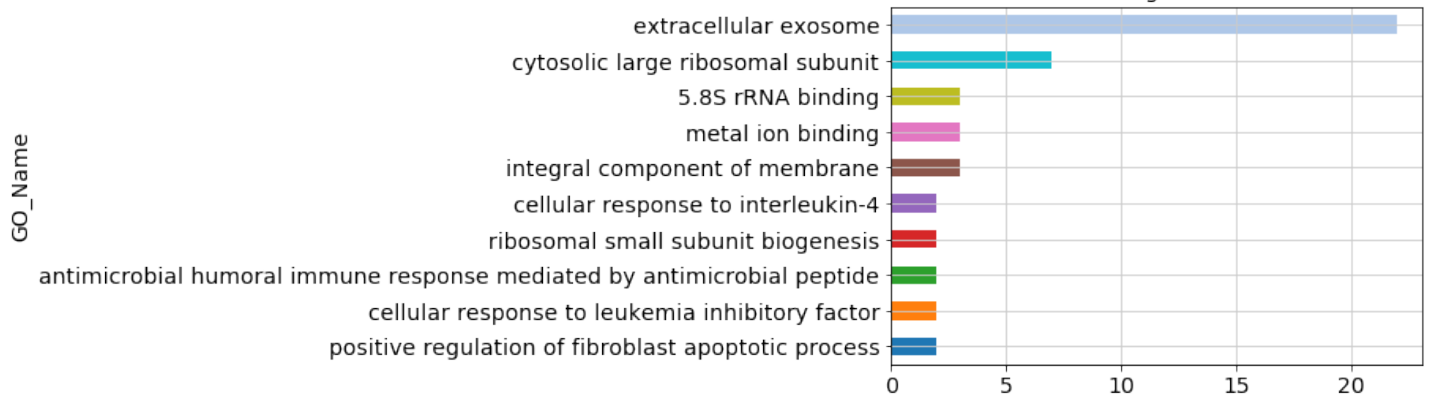
B

Enriched Ontologies in Cluster #1

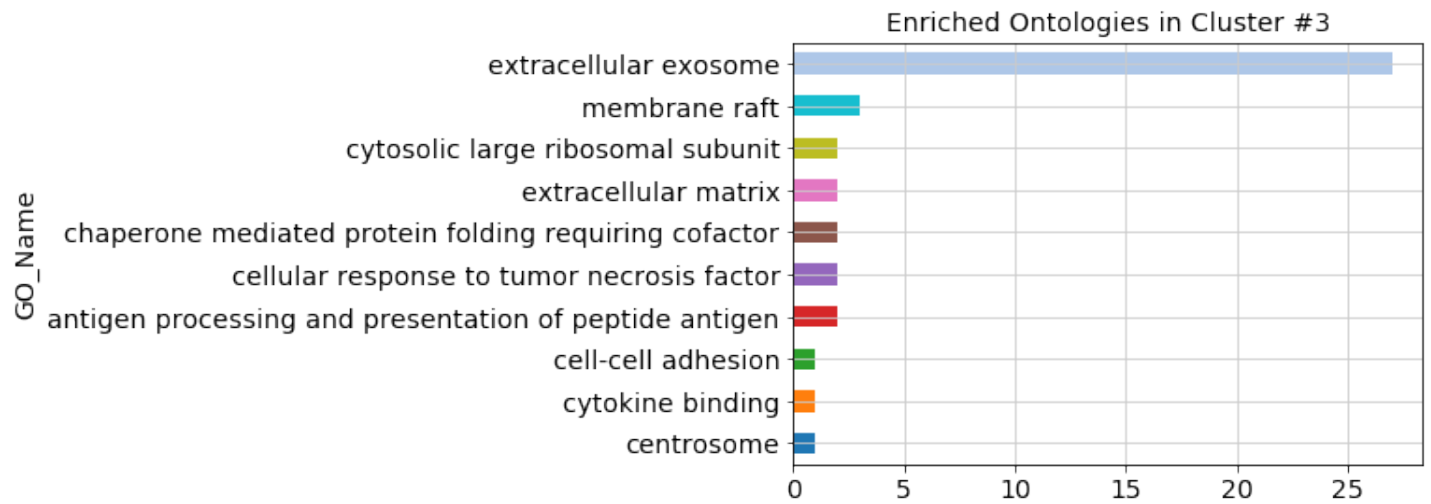


C

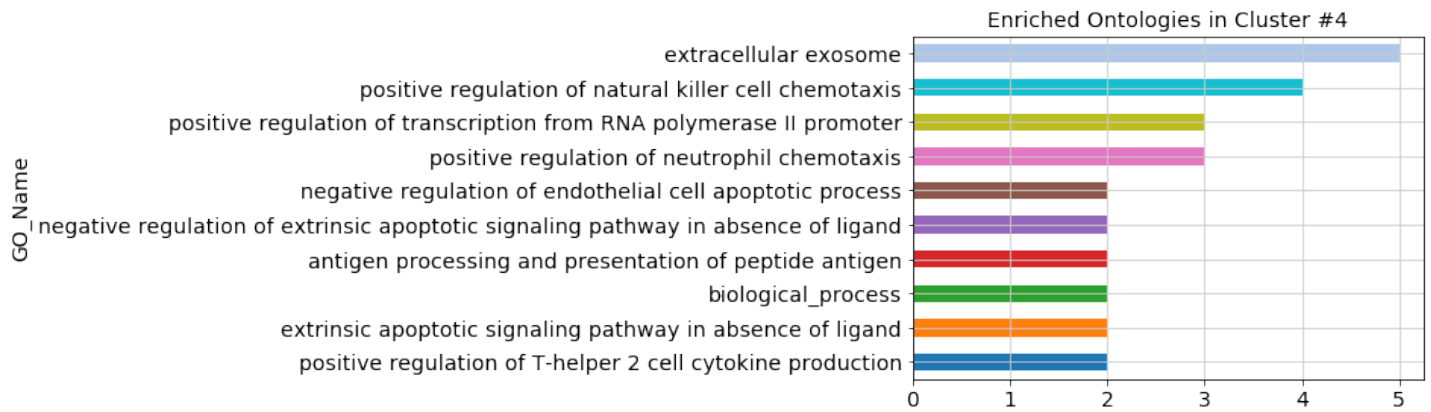
Enriched Ontologies in Cluster #2



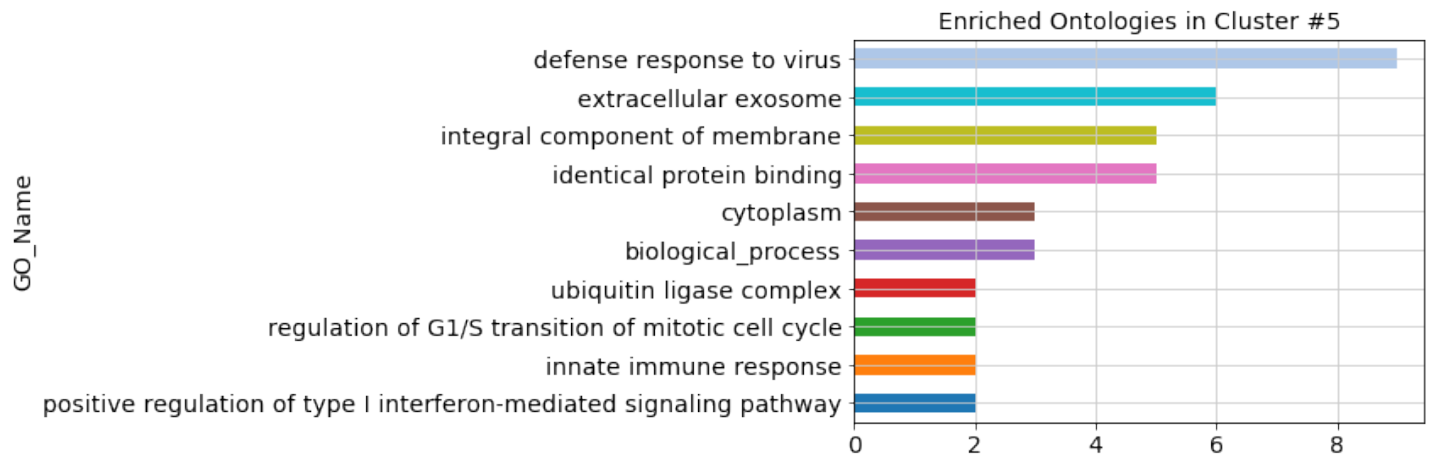
D



E

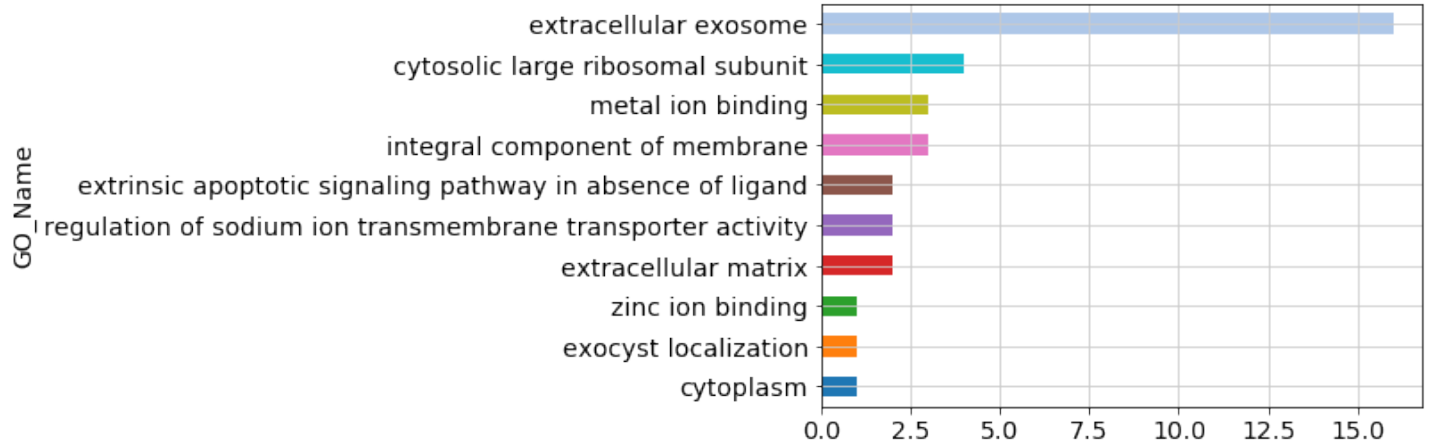


F



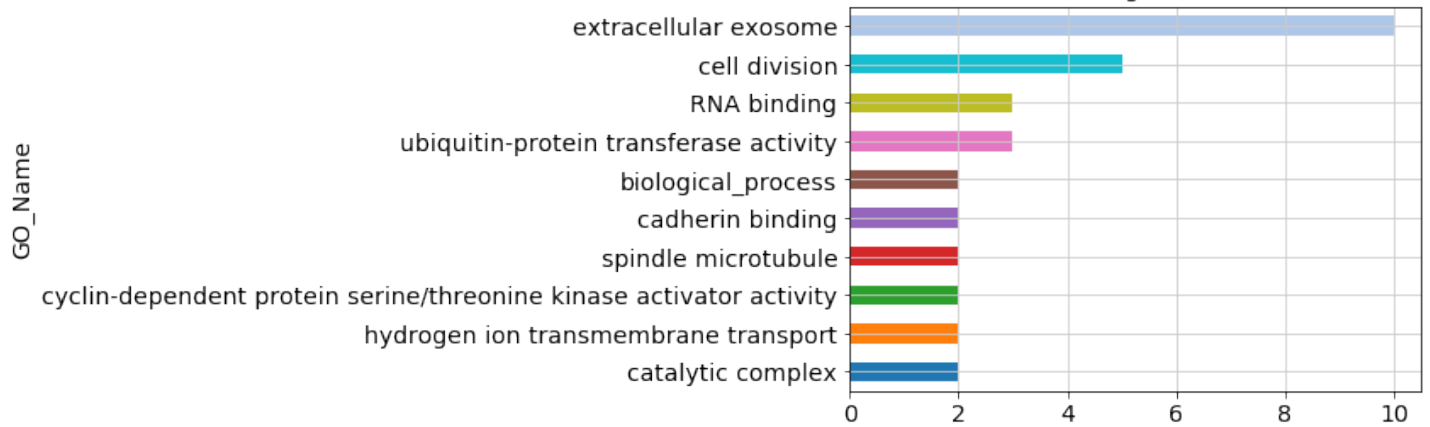
G

Enriched Ontologies in Cluster #6



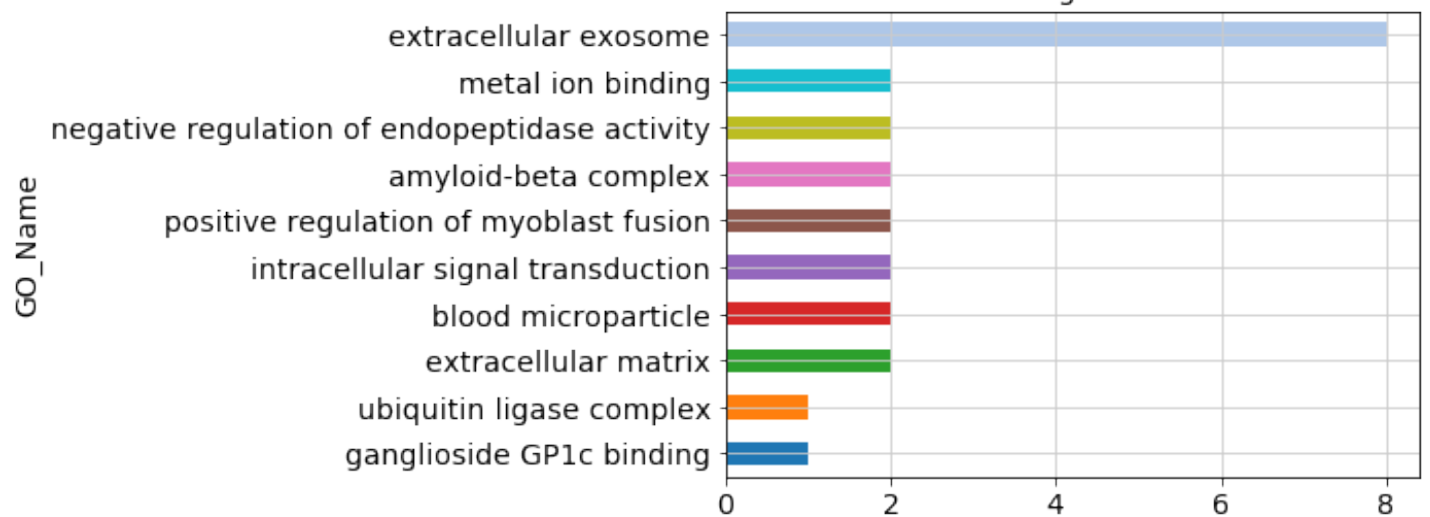
H

Enriched Ontologies in Cluster #7

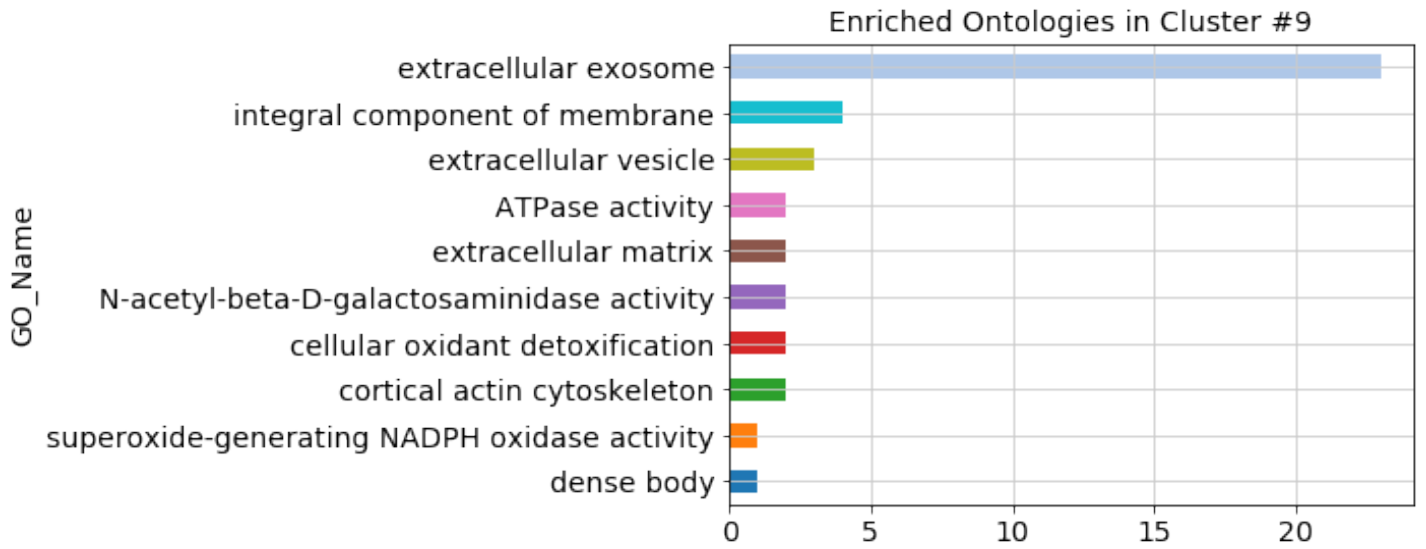


I

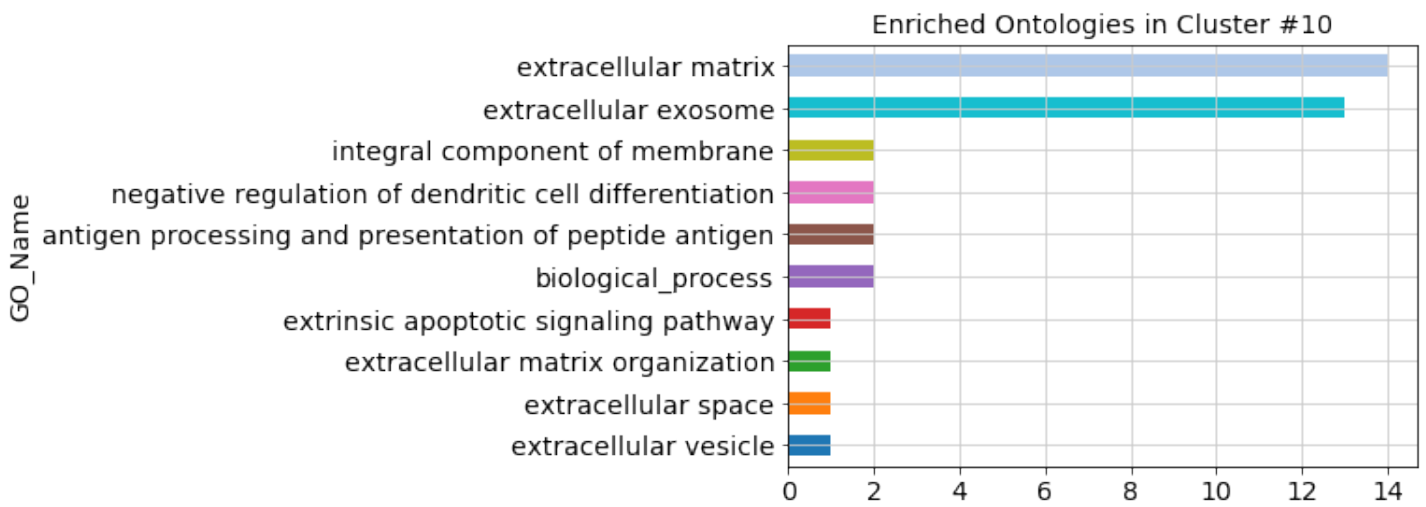
Enriched Ontologies in Cluster #8



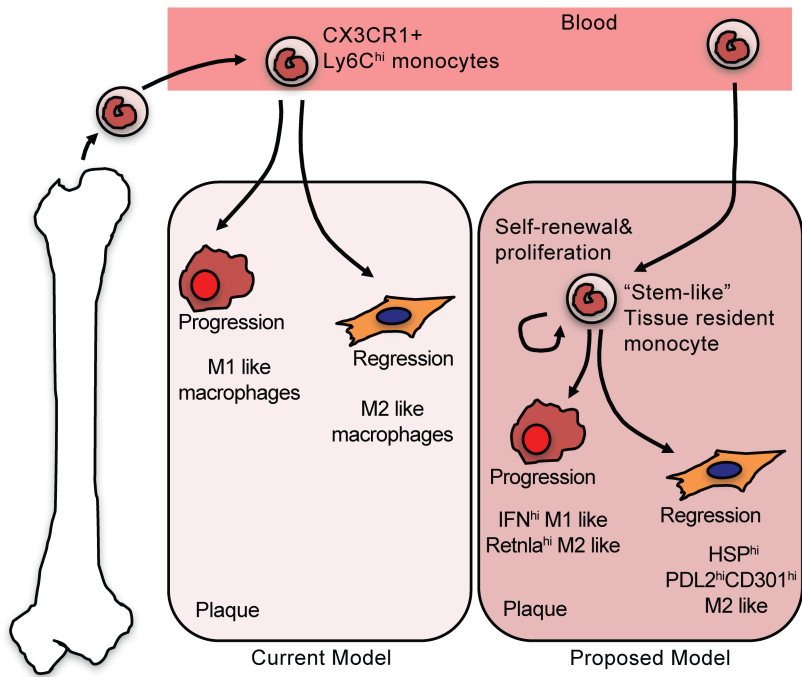
J



K



Supplemental Figure 7. Top 10 gene ontology enrichment analysis in indicted cell Clusters. The top 100 differentially expressed genes from each cell cluster were used to do top 10 gene ontology enrichment analysis in **(A)** Cluster 0; DNase113^{hi} macrophages, **(B)** Cluster 1; Fcrl2^{hi} macrophages, **(C)** Cluster 2; Ebf1^{hi}Cd79a^{hi} macrophages, **(D)** Cluster 3; Retnla^{hi} Ear2^{hi} macrophages, **(E)** Cluster 4; Chemokine^{hi} macrophages, **(F)** Cluster 5; IFN signature^{hi} macrophages, **(G)** Cluster 6; NMES1^{hi} macrophages, **(H)** Cluster 7; Stem-like macrophages, **(I)** Cluster 8; HSP^{hi} macrophages, **(J)** Cluster 9; Trem2^{hi} macrophages, **(K)** Cluster 10; Cd74^{hi}MHCII^{hi} macrophages.



Supplemental Figure 8. Proposed model of monocyte fates in progressing and regressing atherosclerotic plaques based on fate mapping and scRNA-seq results. Taking together previous results by us and others led to a simplified view whereby Ly6C^{hi} monocytes traffic to the plaques and differentiate into either M1-like macrophages during progression or M2-like macrophages during regression. Based on the higher resolution results presented in the present study, we find much greater complexity in macrophage activation states during both atherosclerosis progression and regression (e.g. Trem2^{hi}, Chemokine^{hi}, Fcrl2^{hi}), while some populations are enriched in progression that are both M1-like (IFN signature^{hi}) or M2-like (Retnl^{hi}Ear2^{hi}). Other populations are enriched in regression that are also M2-like (HSP^{hi}, PD-L2^{hi}CD301^{hi}). Notably, we also find a population of stem-like cells that retain CX3CR1 expression and have a proliferative signature that we speculate serve as a reservoir of self-renewing cells that can convert into macrophages of the different phenotypes depending on the plaque microenvironment.

Methods

Mice

B6.*Cx3cr1*^{CreERT2-EYFP/+} mice were generously provided by D. Littman (Skirball Institute of Biomolecular Medicine, NYU Langone Health, New York, NY 10016).

B6.*Rosa26*^{stop-tdTomato} mice (JAX: 007914) and B6.129S7-*LDL*^{rtm1Her}/J mice (JAX: 002207) were from Jackson Laboratories (Bar Harbor, ME). B6.*Cx3cr1*^{CreERT2-EYFP/+} mice and B6.*Rosa26*^{stop-tdTomato} mice were crossed to generate *Cx3cr1*^{CreERT2-EYFP/+} *R26*^{tdTomato/+} mice as previously described (1).

Animals, AAV-mPCSK9, and ApoB-ASO treatment

All animal procedures were approved by the NYU School of Medicine IACUC Committee. Eight week old *Cx3cr1*^{CreERT2-EYFP/+} *R26*^{tdTomato/+} mice were injected intraperitoneally once with AAVmPCSK9 (AAV.8TBGmPCSK9D377Y, Penn Vector Core, using a plasmid originally provided by Dr. Daniel J. Rader) at 10¹² viral particles/mouse and placed onto a Western diet (Dyets Inc., Bethlehem, USA, Dyet #101977) for 18 weeks. At this time point, mice were divided into two groups: continued on Western diet (progression group), switched to a chow diet and injected intraperitoneally twice per week with apolipoprotein B (ApoB) anti-sense

oligonucleotide (ASO) 50mg/kg for two weeks (n = 4-10) to lower levels of atherogenic apoB-containing lipoproteins.

Flow cytometry sorting or analysis

CD11b+TdT⁺ macrophages were isolated using the BD FACS Aria IIu SORP from baseline and regression aortic arches that were removed from mice after perfusion of cold PBS and enzymatic digestion as described in Rahman et al., 2017 (2). After live/dead cell staining with blue reactive dye (catalog#L23105, Invitrogen), cell surface markers were labeled with the following antibodies: CD11b Brilliant Violet 650 (Catalog#101259, Biolegend) or CD11b Buv395 (catalog#563553, BD BioScience), F4/80 PE/Cy7, PDL2 APC, CD301 PerCP/Cy5.5, IA/IE APC/Cy7, CD3 Pacific Blue, CD19 Pacific Blue, CD49b Pacific Blue, Ly6G Brilliant Violet 421, Sca-1 Pacific Blue, CD14 PerCP/Cy5.5, CD9 PE/Cy7, F4/80 BV711, CD45 BV510 (catalog, #123114, #107210, #145710, #107628, #100214, #115523, #108918, #122520, #123314, #124816, #123147, #103137, Biolegend), and Siglec-F Brilliant Violet 421 (catalog#562681, BD BioScience). During cell sorting, cellular debris was excluded with FSC and SSC gating and lymphocytes, eosinophils, and neutrophils were excluded with Pacific Blue and Brilliant Violet 421 positive gating. Sorted CD11b+TdT⁺ cells were processed to single-cell RNA sequencing as described

below. FACS analyses were also performed in ZE5 cell analyzer (BIO-RAD).

Recorded FACS data were analyzed by Flowjo v10.4.2.

Single-cell library construction and sequencing

The sorted CD11b+TdTomato+ cellular suspensions were loaded on a 10x Genomics Chromium instrument to generate single-cell gel beads in emulsion (GEMs).

Approximately 10,000 cells were loaded per channel. Single-cell RNA-Seq libraries were prepared using the following Single Cell 3' Reagent Kits v2: Chromium™

Single Cell 3' Library & Gel Bead Kit v2, Single Cell 3' Chip Kit v2, and i7

Multiplex Kit (catalog# PN-120237, PN-120236, # PN-120262, 10x Genomics) as

described in <https://www.ncbi.nlm.nih.gov/pubmed/28091601>, and following the

Single Cell 3' Reagent Kits v2 User Guide (Manual Part # CG00052), Rev A.

Libraries were run on an Illumina HiSeq 4000 as 2 × 150 paired-end reads, one full

lane per sample, for approximately >90% sequencing saturation.

Alignment, barcode assignment and UMI counting

The Cell Ranger Single Cell Software Suite, version 1.3 was used to perform sample de-multiplexing, barcode and UMI processing, and single-cell 3' gene counting. A

detailed description of the pipeline and specific instructions to run it can be found at:

<https://support.10xgenomics.com/single-cell-gene-expression/software/pipelines/latest/what-is-cell-ranger>

Histology and immuno-fluorescence staining of aortic sections

Aortic roots were removed, perfused with saline and embedded in OCT. Serial sections were cut and fixed in cold acetone for 10 min and endogenous biotin and streptavidin were blocked with Streptavidin/Biotin Blocking Kit (catalog#SP-2002, Vector Laboratories) and Super Block (catalog#AAA-125, ScyTek Laboratories). Sections were then incubated at 4°C overnight with rat anti-mouse CD68 (AbD Serotec, catalog#MCA1957, 1:10), rabbit anti Ki67 (catalog#RM-9106-S1, Lab Vision; now ThermoFisher; 1:100), and chicken anti-GFP (catalog#ab13970, Abcam; 1:200) antibodies in normal antibody diluent (catalog#08980641, MP Biomedicals). Slides were washed in PBS and then incubated at room temperature for 30 mins with biotinylated rabbit-anti-rat IgG mouse-adsorbed secondary antibody (catlog#BA-4001, Vector Laboratories) or UltraTek anti-rabbit biotinylated antibody (catalog#ABK125, ScyTek Laboratories; Ready to Use), followed by a 20 min room temperature incubation with Goat anti-chicken IgY Alexa Fluor 488 conjugated (catalog# ab150169, Abcam; 1:250) and Streptavidin Alexa Fluor 647 conjugated (catalog# S-21374, Abcam; 1:250) antibodies. After immunostaining, tissue sections

were wash in PBS and DAPI counter-staining and mounting with DAPI-Fluoromount-G (catalog#0100-20, Southern Biotech).

Imaging of aortic sections

Bright field images were acquired by a Leica DM4000B microscope and Leica DC300Fx camera using a 4x objective in both brightfield and fluorescence. ImagePro Plus 5.0 software (Media Cybernetics) was used to determine total root area, total plaque percentage per root. Immuno-fluorescence images were acquired by a Nikon Eclipse Ti epifluorescence microscope. Multiple images were taken using an x20 dry objective and tiled together. The imaging data were processed and analyzed using Imaris software version 9.0.1 (Bitplane; Oxford Instruments).

Computational analysis

t-distributed stochastic neighbor embedding (t-SNE) in Flowjo analysis

Flowjo v10.4.2 software and plugin were installed per manufacturer's instructions. Gated CD11b+TdTomato+ cells from aortic arches of progression and regression mice were concatenated into progression and regression groups. Then progression and regression groups were concatenated together and used to perform t-SNE analysis with Flowjo plugin.

Pre-processing Sequencing Data

Using the Cellranger analysis pipeline (*cellranger mkfastq* and *cellranger count*) provided by 10X Genomics FASTQ files were generated and aligned, sequencing data were filtered, and finally, barcodes and UMIs were assigned to each data point in the raw sequencing output. Experiments were then aggregated using Cellranger (*cellranger aggr*) to compare progression and regression experimental groups with normalized sequencing-depth and expression data (<https://support.10xgenomics.com/single-cell-gene-expression/software/pipelines/latest/what-is-cell-ranger>). Initial tSNE Clustering and exploration of differential gene expression were performed using the Loupe™ Cell Browser from 10X Genomics.

Pre-processing was continued using the Scanpy library for Python 3 as in Wolf et al., 2018 (3). The methodology described therein is used throughout the majority of this analysis. To ensure quality of input data, genes expressed in fewer than 3 cells were removed. The steps outlined in (3, 4) were then used in order to remove those cells with excessive mitochondrial gene expression and to normalize the per-cell gene expression values. Gene expression values were transformed by $\ln(1+x)$. In order to prepare the data for Clustering, Scanpy was used to sub-select a collection of genes

with highly variable expression. In order to more accurately calculate differential gene expression, the subsets of highly variable genes were regularized via regression on the mitochondrial gene expression.

Dimensionality Reduction

The JackStraw and elbow plot methodology from the Seurat R package (4-6) was used in order to evaluate the number of statistically significant principal components (PCs) required to accurately describe the variation in the single cell expression data.

This analysis arrived at a liberal estimate of 32 PCs. PCA with was subsequently used in the Clustering and visualization processes in order to accomplish the requisite dimensionality reduction.

Clustering, Visualization, and Feature Extraction

Louvain community detection on the PCA reduced data was used in order to Cluster the single cell observations in an unsupervised manner. Visualization by the t-SNE and UMAP methodologies in the Scanpy package (3, 7-9) allowed for the assessment of the spatial distribution of the Louvain Clusters. The proportion of each Cluster occupied by progression vs. regression experimental group cells was calculated.

Feature Selection and Heat Mapping

Scanpy was harnessed in order to perform One vs Rest statistical testing with the overestimated-variance T-test, allowing for identification of genes that were

significantly overexpressed in each Louvain Cluster. A heatmap was then utilized in order to reveal heterogeneity of expression across the cells sampled, and to visualize the intensity of Cluster-associated gene expression. Each cell lies on the y-axis and the 5-10 genes ranked with the highest differential expression for each Louvain Cluster lie on the x-axis. The intensity of each cell in the heatmap represents the regularized $\ln(1+x)$ gene expression value.

Immgen Analysis

In order to gain insight into the cell types represented in our single-cell sample, a comparison of phenotype was performed against RNA microarray data from the Immgen database (10). Only RNA expression profiles for macrophages, monocytes, and dendritic cells were included. The Immgen microarray reads were first row-normalized to mean 0 and standard deviation of 1. Then, both the Immgen and single cell data was column-normalized to have mean 0 and standard deviation of 1. The number of genes expressing > 1 reads in at least 90% of cells in the Cluster was first established to be 138. The 138 genes with the greatest differential expression (as determined previously) in Cluster7 were then taken and used in our visualization. Not all of the differentially expressed genes were found in the Immgen database; these were dropped (9/138). Duplicate gene expression values were found in the Immgen data, and the median expression levels for these genes were used. The single cells

were randomly grouped into four sub-groups and the median expression of each gene used for display. We heatmap the normalized expression of each Immgen cell-type alongside the 4 sub-groups randomly permuted and aggregated from Cluster 7.

Hierarchical Clustering was then used to rearrange the heatmap rows (to Cluster similar cell types) and potentially also the columns (to show blocks of associated gene expression).

Diffusion Pseudotime Analysis

DPT analysis algorithms from the Scanpy package were employed in order to reconstruct the divergence of cell lineages based upon their proximity on a random-walk (3). We hypothesized that our origin Cluster would contain monocytes with high expression of CX3CR1, so the population of cells with the highest average expression of this gene was determined and the cell among this population with the highest CX3CR1 expression was chosen to be the “root” cell as required by this algorithm.

The data are again prepared by paring it down to 32 PCs using PCA and calculating the 30 nearest neighbors. A diffusion map is then generated, modeling the differentiation trajectory of each cell (3, 11). The diffusion pseudotime value, an estimation of how far in expression each cell is relative to the root cell, is subsequently calculated.

When designating a root cell with high CX3CR1 expression, the cells with the lowest pseudotime values localized to one extreme of the diffusion map trajectory. The lowest pseudotime values localize to the middle of the diffusion map when a low CX3CR1 cell is chosen.

Proliferative Capacity Screening

In order to determine which Louvain Cluster had the greatest capacity to proliferate, the expressions of various cell cycle genes were quantified. Using work by Whitfield et al., 2002 (12), genes associated with the G1/S checkpoint, the S phase, the G2 phase, and the G2/M checkpoint were identified. The expression of these genes was then summed for each cell, and aggregated by Louvain Cluster in order to gain an idea of the proliferative potential of each sub-population.

GO term analysis

We selected top 100 differentially expressed genes per cluster, which had a Z-score > 1.64 (one-tailed $p=0.5$), and then associated those gene names with GO tags.

Differential GO analysis was used by Goatools package

(see <https://www.nature.com/articles/s41598-018-28948-z>).

Comparison of scRNA-seq Data with Previously Published Microarray Data

Transplant regression model. We analyzed the microarray two-color (spot-level) fluorescence intensity data from the Feig et al., 2012 (13) study using the R software package Limma (14). We selected for genes meeting a minimum intensity level by retaining only genes with a sample-mean \log_2 A-value of at least -5.0. We tested for differential expression with empirical Bayes variance estimation and a q -value cutoff of 0.01. We joined the gene-level \log_2 (regression/progression) ratios from the Feig et al. microarray study with the gene-level pseudotime values from the scRNA-seq data from this study using official gene symbols, resulting in the joint pseudotime and \log_2 (regression/progression) values for 53 genes shown in Fig. 5C.

Reversa regression model. We merged gene expression \log_2 (polyI:C/saline) values from the Ramsey et al. 2014 study (15) with gene-level \log_2 (regression/progression) values from supervised analysis of the scRNA-seq data (Limma empirical Bayes test on voom-normalized log-expression data, FDR < 0.01) from the scRNA-seq study using official gene symbols, resulting in the joint values for the 27 genes shown in Fig. 4C.

Comparison and Merge of Our scRNA-seq Dataset to a Published Study

We analyzed a recently published single cell RNA-seq dataset from CD45+ cells from *Ldlr*^{-/-} C57BL/6 aortas (GEO accession number GSM3215435) (Kim et al., 2018 (16)). Using the filtered matrix of gene by cell expression values, we performed

further filtering using the R package Seurat, removing cells with the percentage of genes expressed from the mitochondria greater than 7.5% and more than 5,500 expressed genes based on the overall distribution of the data, yielding data from 3,698 cells. We performed an initial analysis of this dataset alone, also done in Seurat, by performing PCA and using the resulting PCs to find Louvain clusters and perform tSNE dimension reduction. We also performed an analysis merging the Kim et al. data with the progression and regression data that we generated. Following the method outlined in Butler et al. (17), we performed canonical correlation analysis (CCA) and aligned the canonical correlation vectors (CCs) using the R package Seurat. Using the aligned CCs, Louvain clusters were found and tSNE dimension reduction was performed. In both the analysis of the Kim et al data alone and the merged analysis, we calculated the sum of expression from G1/S genes (Ccne1, E2f1, Cdc6, and Pcna), S genes (Rcf4, Dhfr, Rrm2, and Rad51), G2 genes (Cdk1, Top2a, Ccnf, and Ccna2), and G2/M genes (Aurka, Bub1, Ccnb1, Plk1, Plk2, Plk3, and Plk4). We also used the sum of expression of G1/S, S, G2, and G2/M genes as a measure of “stemness”.

Methods References

1. Gundra UM, Girgis NM, Gonzalez MA, San Tang M, Van Der Zande HJP, Lin JD, et al. Vitamin A mediates conversion of monocyte-derived macrophages into tissue-resident macrophages during alternative activation. *Nat Immunol.* 2017;18(6):642-53.
2. Rahman K, Vengrenyuk Y, Ramsey SA, Vila NR, Girgis NM, Liu J, et al. Inflammatory Ly6Chi monocytes and their conversion to M2 macrophages drive atherosclerosis regression. *J Clin Invest.* 2017;127(8):2904-15.
3. Wolf FA, Angerer P, and Theis FJ. SCANPY: large-scale single-cell gene expression data analysis. *Genome Biol.* 2018;19(1):15.
4. Satija R, Farrell JA, Gennert D, Schier AF, and Regev A. Spatial reconstruction of single-cell gene expression data. *Nat Biotechnol.* 2015;33(5):495-502.
5. Haber AL, Biton M, Rogel N, Herbst RH, Shekhar K, Smillie C, et al. A single-cell survey of the small intestinal epithelium. *Nature.* 2017;551(7680):333-9.
6. Macosko EZ, Basu A, Satija R, Nemes J, Shekhar K, Goldman M, et al. Highly Parallel Genome-wide Expression Profiling of Individual Cells Using Nanoliter Droplets. *Cell.* 2015;161(5):1202-14.
7. Becht E, Dutertre C-A, Kwok IWH, Ng LG, Ginhoux F, and Newell EW. Evaluation of UMAP as an alternative to t-SNE for single-cell data. *bioRxiv.* 2018.
8. Leland McInnes JH. arXiv; 2018.
9. Vincent D, Blondel J-LG, Renaud Lambiotte, Etienne Lefebvre. Fast unfolding of communities in large networks. *Journal of Statistical Mechanics: Theory and Experiment.* 2008(10):P10008.
10. Heng TS, and Painter MW. The Immunological Genome Project: networks of gene expression in immune cells. *Nat Immunol.* 2008;9(10):1091-4.
11. Haghverdi L, Buettner F, and Theis FJ. Diffusion maps for high-dimensional single-cell analysis of differentiation data. *Bioinformatics.* 2015;31(18):2989-98.
12. Whitfield ML, Sherlock G, Saldanha AJ, Murray JI, Ball CA, Alexander KE, et al. Identification of genes periodically expressed in the human cell cycle and their expression in tumors. *Mol Biol Cell.* 2002;13(6):1977-2000.
13. Feig JE, Vengrenyuk Y, Reiser V, Wu C, Statnikov A, Aliferis CF, et al. Regression of atherosclerosis is characterized by broad changes in the plaque macrophage transcriptome. *PLoS One.* 2012;7(6):e39790.

14. Ritchie ME, Phipson B, Wu D, Hu Y, Law CW, Shi W, et al. limma powers differential expression analyses for RNA-sequencing and microarray studies. *Nucleic Acids Res.* 2015;43(7):e47.
15. Ramsey SA, Vengrenyuk Y, Menon P, Podolsky I, Feig JE, Aderem A, et al. Epigenome-guided analysis of the transcriptome of plaque macrophages during atherosclerosis regression reveals activation of the Wnt signaling pathway. *PLoS Genet.* 2014;10(12):e1004828.
16. Kim K, Shim D, Lee JS, Zaitsev K, Williams JW, Kim KW, et al. Transcriptome Analysis Reveals Nonfoamy Rather Than Foamy Plaque Macrophages Are Proinflammatory in Atherosclerotic Murine Models. *Circ Res.* 2018;123(10):1127-42.
17. Butler A, Hoffman P, Smibert P, Papalexi E, and Satija R. Integrating single-cell transcriptomic data across different conditions, technologies, and species. *Nat Biotechnol.* 2018;36(5):411-20.